Electrochimica Acta 306 (2019) 360–365

Contents lists available at ScienceDirect

Electrochimica Acta

journal homepage: www.elsevier.com/locate/electacta

Interface-induced controllable synthesis of Cu_2O nanocubes for electroreduction CO_2 to C_2H_4

Wenhang Wang [a], Hui Ning [a, **], Zhongxue Yang [a], Zhaoxuan Feng [a], Jialin Wang [a], Xiaoshan Wang [a], Qinhu Mao [a], Wenting Wu [a], Qingshan Zhao [a], Han Hu [a], Yan Song [b], Mingbo Wu [a, *]

[a] State Key Laboratory of Heavy Oil Processing, Institute of New Energy, College of Chemical Engineering, China University of Petroleum (East China), Qingdao, 266580, China
[b] CAS Key Laboratory of Carbon Materials, Institute of Coal Chemistry, Chinese Academy of Sciences, Taiyuan, 030001, China

ARTICLE INFO

Article history:
Received 29 November 2018
Received in revised form
12 March 2019
Accepted 20 March 2019
Available online 23 March 2019

Keywords:
CO_2 electroreduction
Graphite sheets
Ionic liquid
Ethylene
Cuprous oxide

ABSTRACT

Electroreduction CO_2 to high value-added chemicals is a promising way to mitigate the greenhouse effect while storing the renewable electricity in chemicals. As an important chemical, C_2H_4 is a desirable product of CO_2 reduction but limited by lacking of efficient and durable catalysts. Herein, we proposed an interface-induced method to prepare Cu_2O nanocubes with controllable morphology and size. Due to the imidazolyl groups connected to the surface of ionic liquid functionalized graphite sheets (ILGS), Cu_2O nanocubes were induced to grow on ILGS to obtain Cu_2O/ILGS composites, where the size of Cu_2O can be controlled by adjusting the concentration of Cu^{2+}. Interestingly, as the concentration of Cu^{2+} increases from 12.5 mmol/L to 100 mmol/L, the size of Cu_2O nanocubes decreases from 456 nm to 72 nm. As catalyst for CO_2 electroreduction in 0.1 M $KHCO_3$ aqueous solution, Cu_2O/ILGS-100 (synthesized under 100 mmol/L $CuCl_2$) behaves the best catalysis performance with a high faradic efficiency of C_2H_4 (31.1%) and long durability at −1.15 V (*vs.* reversible hydrogen electrode).

1. Introduction

Electroreduction of carbon dioxide (CO_2RR) to high value-added chemicals offers an opportunity for alleviating the greenhouse effect and storing the renewable electricity in chemicals [1–4]. Recent progresses in electroreduction of CO_2 mainly focus on the production of gaseous carbon products, such as carbon monoxide (CO) [5,6] methane (CH_4) [7,8] and ethylene (C_2H_4) [9,10], of which C_2H_4 is of significant value but limited by lacking of efficient and durable catalysts [11].

Among all the screened materials, copper-based materials have shown the best performance for electrocatalytic CO_2 to hydrocarbons, especially for C_2H_4 [12–15]. Recently, Cu_2O is found to have high selectivity to C_2H_4 in electrocatalytic CO_2RR, whose performance is closely related to its morphology and size [16–20]. Recent research has proved that the surface of Cu_2O is reduced to Cu^0 with O vacancies during the CO_2RR [21], which is greatly affected by the applied potentials and currents [22]. The high C_2H_4 selectivity brought by Cu_2O catalysts is more likely due to a high density of grain boundaries with plenty of unsaturated coordinated copper atom with suitable atomic spacing. Liu et al. [23] proposed a metal embedded in oxidized matrix model with quantum mechanics methods to explain the activity and selectivity of Cu_2O in electrocatalytic CO_2RR, indicating that the Cu_2O matrix plays the key role in maintaining the high performance of oxide derived Cu^0.

As a result, construction of Cu_2O crystals with suitable morphology and size to exposure plenty of unsaturated coordinating Cu atoms are crucial to improving the activity and selectivity of Cu_2O for electrocatalytic CO_2RR to C_2H_4. Unfortunately, the synthesis of well-defined and highly dispersed Cu_2O nanocrystals is still a great challenge. Huang et al. prepared Cu_2O nanocubes by controlling the aggregation of Cu_2O seed particles and surface reconstruction method via sodium dodecyl sulfate as capping surfactant [24]. Yeo et al. reported copper(I) oxide films electrodeposited from an electrolyte of 0.3 mol/L $CuSO_4$, 3.2 mol/L NaOH and 2.3 mol/L Lactic acid in water at various electrochemical potentials [25]. Wang et al. prepared Cu_2O hollow spheres by

* Corresponding author.
** Corresponding author.
E-mail addresses: ninghui@upc.edu.cn (H. Ning), wumb@upc.edu.cn (M. Wu).

https://doi.org/10.1016/j.electacta.2019.03.146
0013-4686/

adjusting the concentration of CTAB in water under 60 °C [26]. These reported methods usually need trivial steps and massive energy consumption, bulk organic solvents or mass surfactants, which are environmentally unfriendly. Therefore, it is of great significance to invent an economic method for controllable synthesis of Cu_2O nanocrystals with high catalytic performance for C_2H_4 production from CO_2RR.

The interface-induced method is an outstanding strategy for controllable preparation of metal materials [27]. Carbon materials generally possess excellent chemical and thermal stabilities, good electrical conductivity [28], and flexible designability, making them promising candidates as supports to synthesize metal based composites based on interface-induced method [29,30]. Pan et al. developed a facile interface-induced Zn(II)-ligand-fragment co-assembly strategy to in situ fabricate boronate-based MOF membrane on hydrophobic porous carbon substrate for specific molecular recognition and separation. A catechol-containing medicinal natural flavone luteolin was found to be efficiently and selectively recognized on the MOF composite in water-containing solution due to the phenylboronic acid groups and carbon substrate [31]. Ren et al. employed the graphene oxide (GO) support to template Cu_2O nanocrystals resulting in well-dispersed Cu_2O nanocrystals that show much promise in photo and chemo-catalytic applications, where GO play roles as the template and a surfactant to achieve dispersed Cu_2O crystals [32]. These preliminary works motivate us to investigate the interface-induced method with carbon materials for controllable synthesis of Cu_2O nanocubes as high efficient catalyst for ethylene production from CO_2RR.

Herein, the ionic liquid functionalized graphite sheets (ILGS) were prepared by electro-exfoliation method according to our previous works [33], which was dispersed into aqueous solution to construct ILGS-water interface. Under the interface effects of ILGS on Cu^{2+}, a series of well-defined Cu_2O nanocubes were in situ fabricated on the surface of ILGS, in which the morphology and size of Cu_2O were completely different with those without ILGS. The as-prepared Cu_2O/ILGS showed significant enhancement of catalytic performance for ethylene formation in CO_2RR.

2. Experiment

2.1. Materials

1-octyl-3-methylimidazolium chloride (OmimCl, 99.0%) was supplied from the Centre of Green Chemistry and Catalysis, LICP, CAS, P. R. China. Copper chloride dihydrate (99.0%), sodium hydroxide (96.0%), potassium hydrogen carbonate (99.5%), ethanol anhydrous (99.7%) and L-ascorbic acid (99.99%) are provided by Sinopharm Chemical Reagent Co., Ltd., P. R. China. Nafion N-117 membranes (0.180 mm thick, ≥0.90 meq·g^{-1} exchange capacity) were purchased from Alfa Aesar China Co., Ltd. High purity graphite rod (ø = 3 mm) was provided by Beijing Crystal Dragon Carbon Technology Co., Ltd., P. R. China. All the reagents are used as received without further treatments. The water was purified by a Millipore system in all experiments.

2.2. Synthesis of Cu_2O/ILGS

Cu_2O/ILGSs were prepared using a simple wet chemical approach. Firstly, ILGS was synthesized according to our previous work [33]. Then, 40 mg ILGS is added into 40 mL water to obtained a well-dispersed suspension under ultrasonic for 30 min at room temperature, denoted as solution A. After that, 12 mL of 12.5 mmol/L $CuCl_2$ aqueous solution was mixed with solution A and stirred vigorously for 1 h, flowing by adding 20 mL of 0.1 mol/L NaOH slowly under stirring to obtain solution B. Subsequently, 50 mL of 6 mmol/L L-ascorbic acid is added to solution B and stirred for 2 h at room temperature. At last, the precipitate was filtered and washed with water and ethanol thoroughly before drying under vacuum at 60 °C for 6 h to obtain a brown power, denoted as Cu_2O/ILGS-12.5. Cu_2O/ILGS-25, Cu_2O/ILGS-50, and Cu_2O/ILGS-100 were prepared with the same procedure except that the concentration of $CuCl_2$ is 25, 50 and 100 mmol/L, respectively. The yields of synthesis method, the nominal and real amount of Cu_2O obtained with the method were listed in Table S1.

As control experiments, pristine Cu_2O-12.5, Cu_2O-25, Cu_2O-50 and Cu_2O-100 were also prepared with the same procedure without adding ILGS in solution A, where the number after the Cu_2O represented the concentration of Cu^{2+} (mmol/L).

2.3. Materials characterization

The morphologies of materials were characterized by scanning electron microscopy (SEM, Hitachi S-4800, Japan). The crystal property and phase composition of all as-prepared materials were investigated by X-ray diffraction (X'Pert PRO MPD, Holland) with Cu Kα radiation at 40 kV and 40 mA with Cu Kα radiation (λ = 1.5406 Å). The surface elemental compositions were recorded by X-ray photoelectron spectroscopy (XPS, Thermo Scientific Escalab 250XI, America) with Al Kα radiation. UV–Vis absorption spectra were measured by a UV–Vis spectrophotometer (UV-2700, SHIMADZU). Thermogravimetric analysis (TGA) was carried on a Shimadzu TA-60Ws thermal analyser (Japan) in air at a ramp rate of 10 °C min^{-1}.

2.4. CO_2RR and product analysis

The CO_2RR was carried out in an H-type electrolytic cell with two compartments, where the anode and cathode were separated by a Nafion 117 proton exchange membrane. A Pt plate (1 × 1 cm^2) and Ag/AgCl electrode (KCl saturated) were used as counter and reference electrode, respectively. Both compartments were filled with 30 mL of 0.1 M $KHCO_3$ as electrolyte. All the working potentials were referred to the reversible hydrogen electrode (RHE) [34]. The pH value of the CO_2 saturated electrolyte is 6.8. All the electrochemical measurements were performed using an electrochemical workstation (CHI 760, Shanghai CH Instruments Co., P. R. China).

The working electrode was fabricated by drop-casting 100 μL of catalyst ink onto a L-type glassy-carbon (GC, ø = 10 mm) and dried with N_2. Before ink deposition, the GC electrode was polished and sonicated in ethanol. The catalyst inks were prepared by dispersing 5.0 mg materials in 10 μL of 5% Nafion solution and 500 μL of ethanol anhydrous.

Before testing, the electrolyte in cathode side was saturated with N_2 for 30 min to exclude air. Then high purity CO_2 (99.999%) was bubbled into the electrolyte for another 30 min. During the electrochemical measurements, the CO_2 gas flow was controlled at 20 mL/min. The gas-phase products generated during CO_2 electrolysis at each fixed potential were collected and quantitatively analyzed by gas chromatograph (BFRL-3420A, China), which was online connected with the head space of the cathodic side of the H-type cell. The gas products were injected to GC using a ten-port valve system with high purity Ar (99.999%) as carrier gas. The GC system was equipped with two columns associating with two detectors. The thermal conductivity detector (TCD) was installed to detect hydrogen and carbon monoxide while the flame ionization detector (FID) was fabricated to detect hydrocarbons. The liquid product was tested with Nash's colorimetric method by UV-Vis spectrophotometer [35]. The faradaic efficiency of all products was calculated according to the methods reported by Yeo et al. [25]

3. Results and discussion

The typical preparation procedure is schematically illustrated in Scheme 1. The XRD patterns (Fig. 1) and XPS spectra (Fig. 2) indicate that Cu_2O nanocrystals are successfully synthesized and in-situ supported on the ILGS. As shown in Fig. 1, the wider diffraction peak at 26.43° is ascribed to the (002) peak of ILGS due to the increased amorphousness and defects after exfoliation of graphite. Other diffraction peaks can be exactly indexed to Cu_2O (JCPDS No.78-2076) at 29.58° (110), 36.44° (111), 42.33° (200), 52.49° (211), 61.40° (220), and 73.56° (311), respectively. No other characteristic peaks exit in the XRD patterns, indicating Cu_2O was successfully synthesized and in-situ supported on ILGS.

It can be seen from the XPS spectra (Fig. 2a) that all Cu_2O/ILGSs are consist of C, N, O and Cu. In Fig. 2b, the peaks at 399.57 eV and 401.06 eV indicate that nitrogen in ILGS is derived from the cations of 1-octyl-3-methylimidazolium chloride, which is used as electrolyte for graphite electro-exfoliation [36]. In Fig. 2c, the characteristic peaks at 932.1 eV and 952.0 eV are corresponding to $Cu2p_{3/2}$ and $Cu2p_{1/2}$, respectively. The specific valence of Cu^+ and Cu^0 was further investigated by Cu LMM Auger spectra (Fig. 2d), the kinetic energy around 916.9 eV confirms the purity of Cu_2O without Cu^0 exiting [37].

SEM images revealed that all the Cu_2O nanocrystals present cubic morphology with obviously different size distributions, as shown in Fig. 3 and Fig. S1. To be specific, obvious cavities on the surface of Cu_2O nanocubes was found in Cu_2O/ILGS-12.5 due to incomplete growing, which is beneficial for the exposure of unsaturated coordinate Cu atoms. The size distribution of Cu_2O nanocubes supported on ILGS showed an abnormal rule in comparison with pristine Cu_2O. As shown in Fig.S2 and Table S2, with the concentration of Cu^{2+} increases from 12.5 mmol/L to 100 mmol/L, the average side length of Cu_2O in Cu_2O/ILGSs decreases from 456 nm to 72 nm, while the average side length of pristine Cu_2O increases from 113 nm to 228 nm, indicating the ILGS can inhibit the growth and aggregation of Cu_2O crystals under high concentration of Cu^{2+}.

The catalytic performances of Cu_2O/ILGSs for CO_2 electroreduction to C_2H_4 were investigated with CO_2-saturated 0.1 M $KHCO_3$ solution as electrolyte in an H-type cell under series potentials. The faradic efficiency of C_2H_4 and other gas products were depicted in Fig. 4. For all Cu_2O/ILGSs, the optimum values of faradaic efficiency for C_2H_4 are at −1.15 V (*vs.* RHE). Cu_2O/ILGS-100 shows a maximum faradaic efficiency (FE) of 31.1% for C_2H_4 products. As shown in Fig. S3, formate as the only liquid product was detected with a combined FE of ca. 100% with gas products for Cu_2O/ILGS-100.

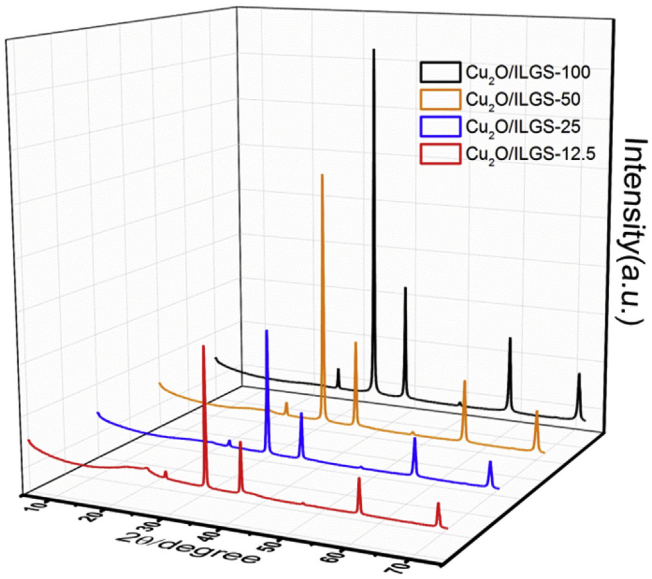

Fig. 1. XRD patterns of Cu_2O/ILGSs.

In our previous work, ILGS has been proved to have no catalytic activity for electroreduction of CO_2 while Cu_2O is the main active sites. For pristine Cu_2O (Fig. 4e), along with the average size of Cu_2O increasing from 113 nm to 228 nm, the FE_{C2H4} declines from 17.5% to 13.8%. Similar trends can also be found for Cu_2O/ILGS-25, Cu_2O/ILGS-50 and Cu_2O/ILGS-100. Reasonably, the highest FE_{C2H4} (31.1%) was obtained over Cu_2O/ILGS-100 due to the smallest size of Cu_2O nanocubes (72 nm). Specially, the FE of C_2H_4 on Cu_2O/ILGS-12.5 is 25.5%, which is close to Cu_2O/ILGS-25 (25.0%), though the size of Cu_2O in Cu_2O/ILGS-12.5 is much larger than that in Cu_2O/ILGS-25. This special phenomenon is corresponding to the special morphology of Cu_2O with obviously cavities on the crystal surface (Fig. 3a), which may arise from the interface-induced effects of ILGS associating with the low concentration of Cu^{2+}. These concavities increase the density of grain boundaries of Cu_2O nanocubes with more unsaturated copper atoms exposed, which is conducive to enhancing the selectivity of C_2H_4 [38]. Among all the materials as made, the Cu_2O nanocubes in Cu_2O/ILGS-100 have the largest loading of 77.6 wt% (Fig. S4, Table S3) and the smallest size of 72 nm, indicating this is a facile method for rapid synthesis of smaller Cu_2O nanocubes using high concentrations of Cu^{2+} for industrial applications.

It is worth noting the mass activity of Cu_2O towards ethylene

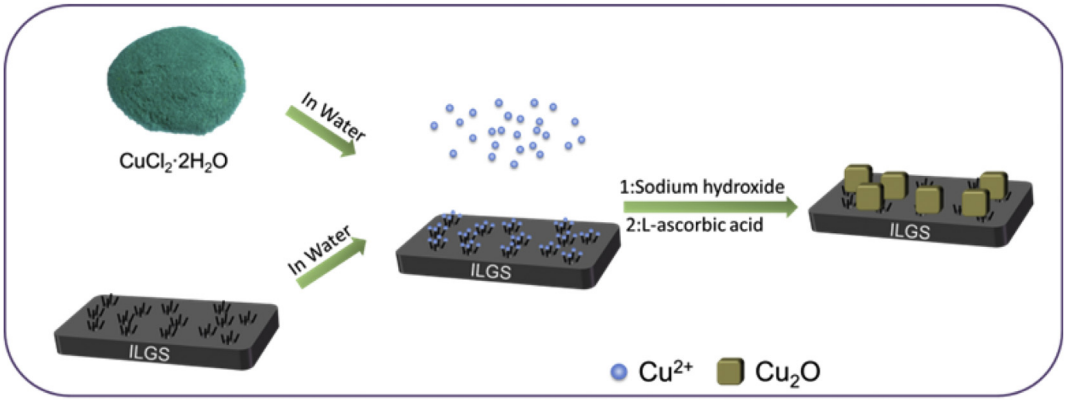

Scheme. 1. Illustration for preparation of Cu_2O/ILGS.

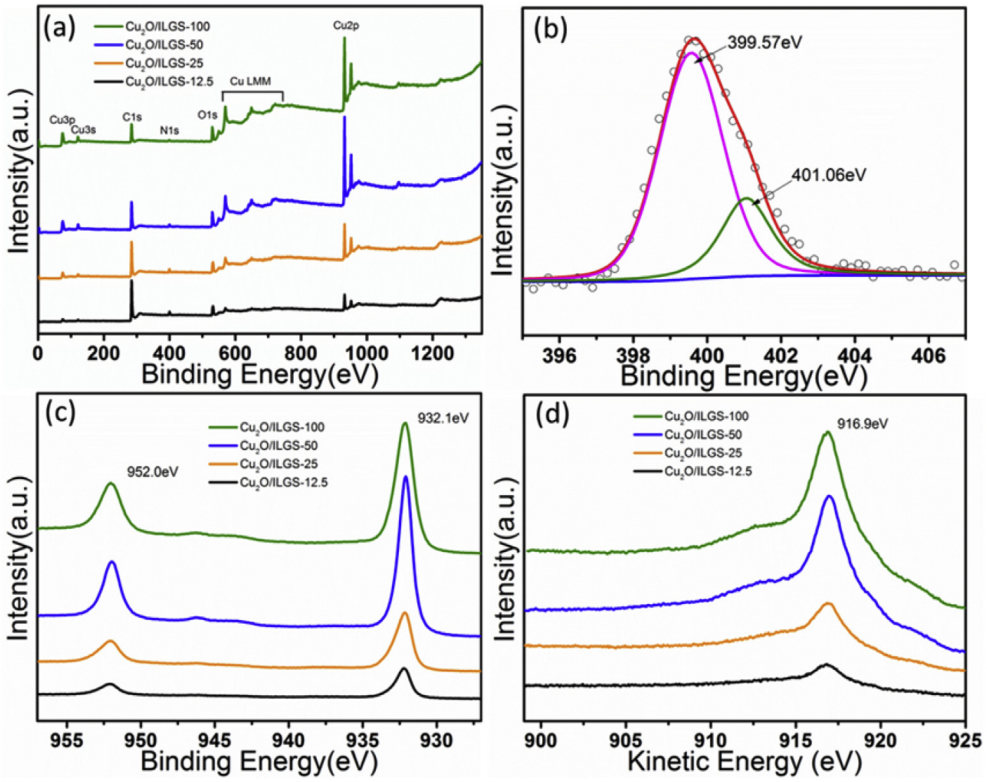

Fig. 2. (a) XPS spectra of Cu_2O/ILGSs, (b) High-resolution N1s spectra of Cu_2O/ILGS-12.5, (c) High-resolution Cu2p spectra of Cu_2O/ILGSs, (d) Cu LMM Auger spectra of Cu_2O/ILGSs.

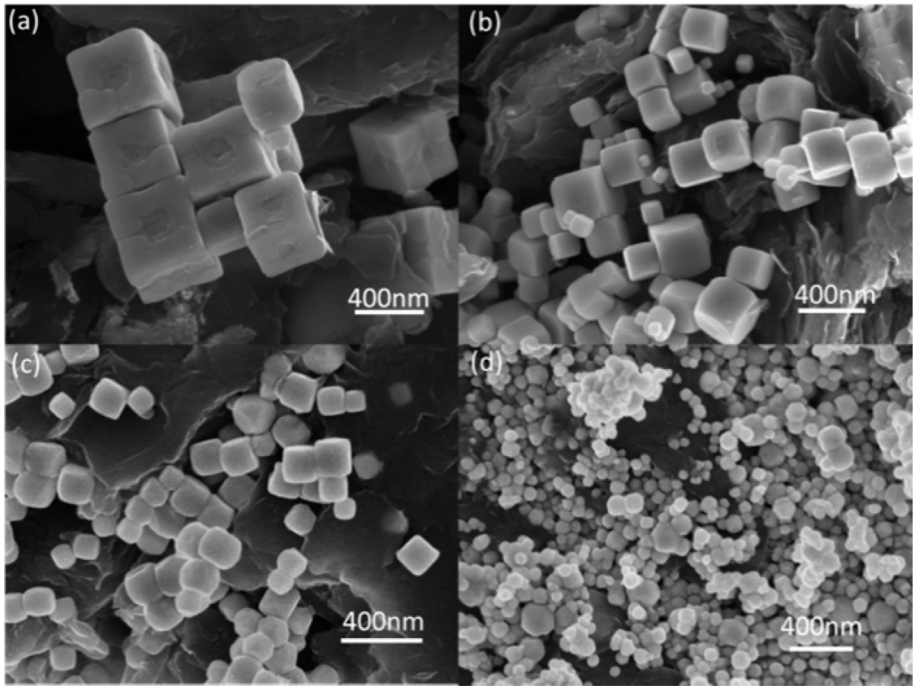

Fig. 3. SEM images of (a) Cu_2O/ILGS-12.5, (b) Cu_2O/ILGS-25, (c) Cu_2O/ILGS-50, (d) Cu_2O/ILGS-100.

formation is meaningful for evaluating the real catalytic activity of copper. Under the optimum potential −1.15 V (*vs.* RHE), the formation rate of ethylene on unit mass of Cu_2O was calculated, as shown in Fig. S5. Not surprisingly, Cu_2O/ILGS-12.5 presents the best performance due to its lowest loading of Cu_2O with obvious concavities, flowing by Cu_2O/ILGS-25 and Cu_2O/ILGS-50. Interestingly, Cu_2O/ILGS-100 exits a relative high yield of C_2H_4, much better than Cu_2O/ILGS-50 and Cu_2O/ILGS-25, with the highest Cu_2O loading. With further to explain this phenomenon, the BET surface area of different materials as-made was calculated according to N_2

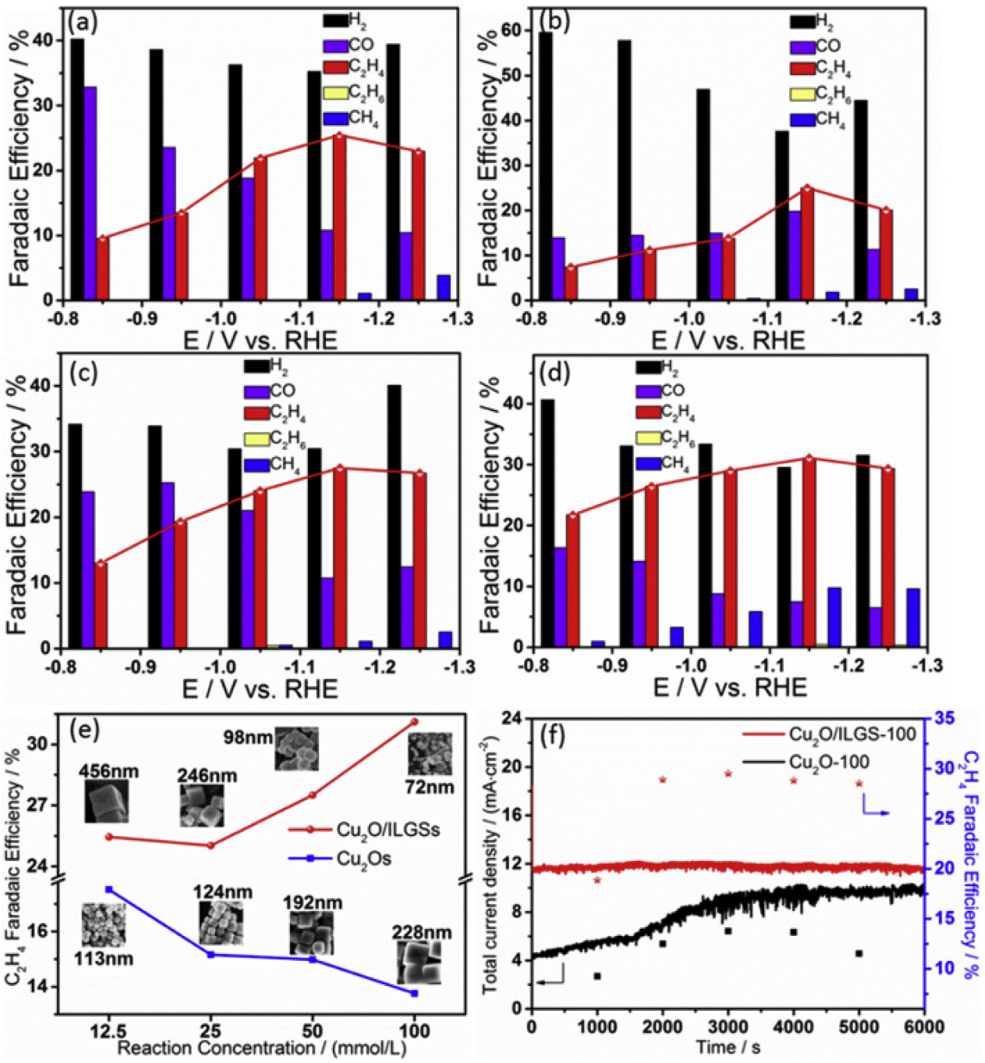

Fig. 4. Faradaic efficiencies of gas products from CO_2RR on (a) Cu_2O/ILGS-12.5, (b) Cu_2O/ILGS-25, (c) Cu_2O/ILGS-50, (d) Cu_2O/ILGS-100. (e) Comparison of FE_{C2H4} on Cu_2O/ILGSs and Cu_2Os at −1.15 V (*vs.* RHE). The insets illustrate the morphology and size of Cu_2O. (f) Stability test of Cu_2O/ILGS-100 and Cu_2O-100 at −1.15 V (*vs.* RHE).

adsorption-desorption isotherms. As depicted in Fig. S6, the BET surface area of Cu_2O/ILGS-12.5, Cu_2O/ILGS-25, Cu_2O/ILGS-50 and Cu_2O/ILGS-100 is 5.90, 5.23, 6.07, and 6.30 $m^2 g^{-1}$, respectively, which is closely related to the size and morphology of Cu_2O nanoparticles. Cu_2O/ILGS-100 has the largest specific surface area due to its smallest size of Cu_2O crystals. However, Cu_2O/ILGS-12.5 has a larger specific surface area than Cu_2O/ILGS-25, even though the latter has a much smaller size of Cu_2O. This is consistent with the special morphology of Cu_2O crystals in Cu_2O/ILGS-12.5, which have obvious surface cavities (Fig. 3a). As revealed by the linear sweep voltammetry (LSV) curve in Fig. S7a, Cu_2O/ILGS-100 achieved the highest total current density from −0.85 V to −1.3 V (*vs.* RHE). According to the mass content of Cu supported on ILGS, the mass-specific current density of all the catalysts was tested and normalized by 1.0 mg copper, as shown in Fig. S7b. It is found that Cu_2O/ILGS-100 still has the largest current density under the measured potentials, indicating that ILGS as supports facilitate the utilization of Cu atom as catalyst for CO_2 electroreduction.

In the end, the stabilities of Cu_2O/ILGS-100 and Cu_2O/ILGS-12.5 were selected as representative samples to investigated the durability of Cu_2O under −1.15 V (*vs.* RHE), as depicted in Fig. 4f and Fig. S8, respectively. Despite the great difference of Cu_2O nanocubes in size and morphology, both Cu_2O/ILGS-100 and Cu_2O/ILGS-12.5 showed better durability than the corresponding pristine Cu_2O, indicating the interface-induced method is preferable to synthesize Cu_2O materials with higher selectivity and better durability for electrocatalytic reduction of CO_2 towards C_2H_4. We further explored the morphology and state of Cu_2O after CO_2 electroreduction. Taking Cu_2O/ILGS-100 for example, the edge of Cu_2O nanocubes is blurred (Fig. S9), indicating the morphology of Cu_2O is not stable during the CO_2 electroreduction [39]. As shown in Fig. S10, the Cu 2p XPS showed that Cu^+ or Cu^0 exists in Cu_2O/ILGS-100 and no Cu^{2+} peaks were observed. With further analyzed form the Auger Cu LMM line (Fig. S11), it is concluded that only minimal Cu^+ was reduced to Cu^0 under the applied negative potential and Cu^+ is still the main active species in Cu_2O/ILGS-100, which play the key role in selectively catalytic CO_2RR to ethylene [19].

4. Conclusions

In summary, an interface-induced method was developed to synthesize Cu_2O nanocubes with controllable morphology and size. Due to the nanostructured surface functionalities of ILGS, Cu_2O nanocubes with smaller size and high loading amount on ILGS were prepared. As the concentration of Cu^{2+} decreases from 100 mmol/L to12.5 mmol/L, the size of Cu_2O on ILGS increases from 72 nm to

456 nm, while the size of pristine Cu_2O without ILGS as supports decreases from 228 nm to 113 nm. This abnormal phenomenon was ascribed to the interface effects of ILGS: (1) The Cu_2O nucleus is preferable to generate on the surface of ILGS rather than in the bulk solution due to the absorption effect of ILGS to Cu^{2+}; (2) The nanostructures of ILGS can fix the position of Cu_2O crystals and inhibit their aggregation. Under the optimal potential for C_2H_4 formation (−1.15 V *vs.* RHE), all Cu_2O/ILGSs show higher selectivity towards C_2H_4 than the corresponding pristine Cu_2O prepared with the same concentration of Cu^{2+}, of which Cu_2O/ILGS-100 exhibits the highest faradic efficiency of ethylene (31.1%). The high performance of Cu_2O/ILGS-100 is attributed to its larger electrochemically active surface area than Cu_2O/ILGS-50, Cu_2O/ILGS-12.5 and Cu_2O/ILGS-25. It is worth noting that Cu_2O nanocubes in Cu_2O/ILGS-100 present the smallest size of 72 nm and the highest loading amount of 77.6 wt%, indicating this interface-induced method has a great potential in scaling up synthesis of small size of Cu_2O with high concentrations of Cu^{2+}. This work not only paves the way for scale preparation of well-defined Cu_2O nanocubes as efficient catalyst for green synthesis of ethylene from CO_2RR, but also enlightens a facile way to control the morphology and size of metal oxides for various electrochemical applications.

Acknowledgements

This work is financially supported by the National Natural Science Foundation of China (Nos. 21808242, 51572296); the Natural Science Foundation of Shandong Province (ZR2018BB070), the Financial Support from Taishan Scholar Project (No. ts201712020).

Appendix A. Supplementary data

Supplementary data to this article can be found online at https://doi.org/10.1016/j.electacta.2019.03.146.

References

[1] M. He, Y. Sun, B. Han, Green carbon science: scientific basis for integrating carbon resource processing, utilization, and recycling, Angew. Chem. Int. Ed. 52 (2013) 9620–9633.
[2] X. Chang, T. Wang, J. Gong, CO_2 photo-reduction: insights into CO_2 activation and reaction on surfaces of photocatalysts, Energy Environ. Sci. 9 (2016) 2177–2196.
[3] Y. Wang, J. Liu, Y. Wang, A.M. Al-Enizi, G. Zheng, Tuning of CO_2 reduction selectivity on metal electrocatalysts, Small 13 (2017) 1701809.
[4] A. Vasileff, C. Xu, Y. Jiao, Y. Zheng, S.-Z. Qiao, Surface and interface engineering in copper-based bimetallic materials for selective CO_2 electroreduction, Chem 4 (2018) 1809–1831.
[5] F. Li, M. Xue, G.P. Knowles, L. Chen, D.R. MacFarlane, J. Zhang, Porous nitrogen-doped carbon derived from biomass for electrocatalytic reduction of CO_2 to CO, Electrochim. Acta 245 (2017) 561–568.
[6] L. Jin, B. Liu, P. Wang, H. Yao, L.A. Achola, P. Kerns, A. Lopes, Y. Yang, J. Ho, A. Moewes, Y. Pei, J. He, Ultrasmall Au nanocatalysts supported on nitrided carbon for electrocatalytic CO_2 reduction: the role of the carbon support in high selectivity, Nanoscale 10 (2018) 14678–14686.
[7] X. Liu, H. Yang, J. He, H. Liu, L. Song, L. Li, J. Luo, Highly active, durable ultrathin $MoTe_2$ layers for the electroreduction of CO_2 to CH_4, Small 14 (2018) 1704049.
[8] X. Sun, X. Kang, Q. Zhu, J. Ma, G. Yang, Z. Liu, B. Han, Very highly efficient reduction of CO_2 to CH_4 using metal-free N-doped carbon electrodes, Chem. Sci. 7 (2016) 2883–2887.
[9] A. Loiudice, P. Lobaccaro, E.A. Kamali, T. Thao, B.H. Huang, J.W. Ager, R. Buonsanti, Tailoring copper nanocrystals towards C_2 products in electrochemical CO_2 reduction, Angew. Chem. Int. Ed. 128 (2016) 5883–5886.
[10] D. Wu, C. Dong, D. Wu, J. Fu, H. Liu, S. Hu, Z. Jiang, S.-Z. Qiao, X.-W. Du, Cuprous ions embedded in ceria lattice for selective and stable electrochemical reduction of carbon dioxide to ethylene, J. Mater. Chem. 6 (2018) 9373–9377.
[11] F.S. Roberts, K.P. Kuhl, A. Nilsson, High selectivity for ethylene from carbon dioxide reduction over copper nanocube electrocatalysts, Angew. Chem. Int. Ed. 54 (2015) 5179–5182.
[12] H. Xie, T. Wang, J. Liang, Q. Li, S. Sun, Cu-based nanocatalysts for electrochemical reduction of CO_2, Nano Today 21 (2018) 41–54.
[13] Y. Hori, K. Kikuchi, S. Suzuki, Production of CO and CH_4 in electrochemical reduction of CO_2 at metal electrodes in aqueous hydrogen carbonate solution, Chem. Lett. 14 (1985) 1695–1698.
[14] Y. Jiao, Y. Zheng, P. Chen, M. Jaroniec, S. Qiao, Molecular scaffolding strategy with synergistic active centers to facilitate electrocatalytic CO_2 reduction to hydrocarbon/alcohol, J. Am. Chem. Soc. 139 (2017) 18093–18100.
[15] C.F.C. Lim, D.A. Harrington, A.T. Marshall, Effects of mass transfer on the electrocatalytic CO_2 reduction on Cu, Electrochim. Acta 238 (2017) 56–67.
[16] C.W. Lee, K.D. Yang, D.H. Nam, J.H. Jang, N.H. Cho, S.W. Im, K.T. Nam, Defining a materials database for the design of copper binary alloy catalysts for electrochemical CO_2 conversion, Adv. Mater. 30 (2018) 1704717.
[17] P.D. Luna, R. Quintero-Bermudez, C. Dinh, M.B. Ross, O.S. Bushuyev, P. Todorović, T. Regier, S.O. Kelley, P. Yang, E.H. Sargent, Catalyst electroredeposition controls morphology and oxidation state for selective carbon dioxide reduction, Nat. Catal. 1 (2018) 103–110.
[18] Y. Chen, C.W. Li, M.W. Kanan, Aqueous CO_2 reduction at very low overpotential on oxide-derived Au nanoparticles, J. Am. Chem. Soc. 134 (2012) 19969–19972.
[19] C. Chen, X. Sun, L. Lu, D. Yang, J. Ma, Q. Zhu, Q. Qian, B. Han, Efficient electroreduction of CO_2 to C_2 products over B-doped oxide-derived copper, Green Chem. 20 (2018) 4579–4583.
[20] A. Eilert, F. Cavalca, F.S. Roberts, J. Osterwalder, C. Liu, M. Favaro, E.J. Crumlin, H. Ogasawara, D. Friebel, L.G. Pettersson, A. Nilsson, Subsurface oxygen in oxide-derived copper electrocatalysts for carbon dioxide reduction, J. Phys. Chem. Lett. 8 (2017) 285–290.
[21] Y. Lum, J.W. Ager, Stability of residual oxides in oxide-derived copper catalysts for electrochemical CO_2 reduction investigated with ^{18}O labeling, Angew. Chem. Int. Ed. 57 (2018) 551–554.
[22] D. Ren, J. Fong, B.S. Yeo, The effects of currents and potentials on the selectivities of copper toward carbon dioxide electroreduction, Nat. Commun. 9 (2018) 925.
[23] D. Kim, C.S. Kley, Y. Li, P. Yang, Copper nanoparticle ensembles for selective electroreduction of CO_2 to C_2-C_3 products, Proc. Natl. Acad. Sci. Unit. States Am. 114 (2017) 10560–10565.
[24] C.H. Kuo, C.H. Chen, M.H. Huang, Seed-mediated synthesis of monodispersed Cu_2O nanocubes with five different size ranges from 40 to 420 nm, Adv. Funct. Mater. 17 (2007) 3773–3780.
[25] D. Ren, Y. Deng, A.D. Handoko, C.S. Chen, S. Malkhandi, B.S. Yeo, Selective electrochemical reduction of carbon dioxide to ethylene and ethanol on copper(i) oxide catalysts, ACS Catal. 5 (2015) 2814–2821.
[26] H. Xu, W. Wang, Template synthesis of multishelled Cu_2O hollow spheres with a single-crystalline shell wall, Angew. Chem. Int. Ed. 46 (2007) 1489–1492.
[27] Z. Zuo, Y. Wen, S. Zhang, Interface-induced nucleation and growth: a new route for fabricating ordered silver nanohole arrays, Nanoscale 10 (2018) 14039–14046.
[28] M. Ding, F. Du, B. Liu, Z.Y. Leong, L. Guo, F. Chen, A. Baji, H.Y. Yang, Rod-like nitrogen-doped carbon hollow shells for enhanced capacitive deionization, FlatChem 7 (2018) 10–17.
[29] J. Yuan, W. Zhi, L. Liu, M. Yang, H. Wang, J. Lu, Electrochemical reduction of CO_2 at metal-free N-functionalized graphene oxide electrodes, Electrochim. Acta 282 (2018) 694–701.
[30] L. Qu, Y. Liu, J. Baek, L. Dai, Nitrogen-doped graphene as efficient metal-free electrocatalyst for oxygen reduction in fuel cells, ACS Nano 4 (2010) 1321–1326.
[31] S. Liu, S. Shinde, J. Pan, Y. Ma, Y. Yan, G. Pan, Interface-induced growth of boronate-based metal-organic framework membrane on porous carbon substrate for aqueous phase molecular recognition, Chem. Eng. J. 324 (2017) 216–227.
[32] C. Hong, X. Jin, J. Totleben, J. Lohrman, E. Harak, B. Subramaniam, R.V. Chaudharib, S. Ren, Graphene oxide stabilized Cu_2O for shape selective nanocatalysis, J. Mater. Chem. 2 (2014) 7147–7151.
[33] H. Ning, W. Wang, Q. Mao, S. Zheng, Z. Yang, Q. Zhao, M. Wu, Catalytic electroreduction of CO_2 to C_2H_4 using Cu_2O supported on 1-Octyl-3-methylimidazole functionalized graphite sheets, Acta Phys. - Chim. Sin. 34 (2018) 938–944.
[34] T.T. Zhuang, Z.Q. Liang, A. Seifitokaldani, Y. Li, P.D. Luna, T. Burdyny, F. Che, F. Meng, Y. Min, R. Quintero-Bermudez, C.T. Dinh, Y. Pang, M. Zhong, B. Zhang, J. Li, P.N. Chen, X.L. Zheng, H. Liang, W.N. Ge, B.J. Ye, D. Sinton, S.H. Yu, E.H. Sargent, Steering post-C-C coupling selectivity enables high efficiency electroreduction of carbon dioxide to multi-carbon alcohols, Nature Catal 1 (2018) 421–428.
[35] J. Hong, W. Zhang, J. Ren, R. Xu, Photocatalytic reduction of CO_2: a brief review on product analysis and systematic methods, Anal. Methods 5 (2013) 1086.
[36] N. Liu, F. Luo, H. Wu, Y. Liu, C. Zhang, J. Chen, One-step ionic-liquid-assisted electrochemical synthesis of ionic-liquid-functionalized graphene sheets directly from graphite, Adv. Funct. Mater. 18 (2008) 1518–1525.
[37] S.Y. Lee, H. Jung, N.K. Kim, H.S. Oh, B.K. Min, Y.J. Hwang, Mixed copper states in anodized Cu electrocatalyst for stable and selective ethylene production from CO_2 Reduction, J. Am. Chem. Soc. 140 (2018) 8681–8689.
[38] Y. Huo, X. Peng, X. Liu, H. Li, J. Luo, High selectivity toward C_2H_4 production over Cu particles supported by butterfly-wing-derived carbon frameworks, ACS Appl. Mater. Interfaces 10 (2018) 12618–12625.
[39] P. Grosse, D. Gao, F. Scholten, I. Sinev, H. Mistry, B. Roldan Cuenya, Dynamic changes in the structure, chemical state and catalytic selectivity of Cu nanocubes during CO_2 electroreduction: size and support effects, Angew. Chem. Int. Ed. 57 (2018) 6192–6197.